PAPER

Check for updates

Thermal reduction of ceria nanostructures on rhodium(111) and re-oxidation by CO_2†

Andreas Schaefer, [ID] *[ab] Benjamin Hagman,[b] Jan Höcker,[cd] Uta Hejral,[b] Jan Ingo Flege [ID] [cd] and Johan Gustafson[b]

The thermal reduction of cerium oxide nanostructures deposited on a rhodium(111) single crystal surface and the re-oxidation of the structures by exposure to CO_2 were investigated. Two samples are compared: a rhodium surface covered to $\approx 60\%$ by one to two O–Ce–O trilayer high islands and a surface covered to $\approx 65\%$ by islands of four O–Ce–O trilayer thickness. Two main results stand out: (1) the thin islands reduce at a lower temperature (870–890 K) and very close to Ce_2O_3, while the thicker islands need higher temperature for reduction and only reduce to about $CeO_{1.63}$ at a maximum temperature of 920 K. (2) Ceria is re-oxidized by CO_2. The rhodium surface promotes the re-oxidation by splitting the CO_2 and thus providing atomic oxygen. The process shows a clear temperature dependence. The maximum oxidation state of the oxide reached by re-oxidation with CO_2 differs for the two samples, showing that the thinner structures require a higher temperature for re-oxidation with CO_2. Adsorbed carbon species, potentially blocking reactive sites, desorb from both samples at the same temperature and cannot be the sole origin for the observed differences. Instead, an intrinsic property of the differently sized CeO_x islands must be at the origin of the observed temperature dependence of the re-oxidation by CO_2.

1 Introduction

The oxides of cerium are essential materials in the chemical industry.[1,2] They are mainly employed as support for metal nanoparticles in heterogeneous catalysis facilitating the oxidation of poisonous CO and removal of nitric gases from, for example, automotive exhaust. The role of cerium oxide, however, exceeds the one of a bare oxide support. Cerium's capability to easily switch between the Ce^{3+} and Ce^{4+} oxidation state results in a high oxygen mobility and storage capacity of the oxide. Hence, catalysts based on cerium oxide have, for example, also been of increasing interest for soot oxidation in the exhaust of diesel engines.[3] In recent years, research has yielded a number of ceria based model catalyst systems that can potentially play an essential role in the future. Especially in

light of the challenges we are facing in terms of energy generation and storage, and increasing levels of atmospheric CO_2, research and development of new materials and concepts is crucial, including research providing a basic understanding of the mechanisms at play on an atomic scale. By studying cerium oxide thin films and nanostructures supported on metal surfaces, so-called inverse catalysts,[4,5] interesting model systems for important reactions could be realized, that can potentially exceed the performance of materials currently employed industrially. Examples for such reactions are the water–gas shift, alcohol reforming, CO_2 hydrogenation to methanol, and methane activation, to name a few.[6]

A prominent example that has received considerable attention is the synthesis of methanol from CO_2 and CO over Cu/ZnO based catalysts. The structure and composition in the active state of the catalyst has been debated, but recent results show that a ZnO layer forms on top of the metal particles of a real catalyst generating a metal–oxide interface that is crucial for the reaction.[7] This strong metal support interaction (SMSI) forming the oxide layer not only affects the structure of the metal particle but also generates a synergistic effect that drives the reaction.[8–10] Furthermore, ceria structures on copper have been shown to achieve even higher turnover rates than the ZnO/Cu system.[11] These results are a strong motivation for the study of inverse configurations, as they might be of importance also in other catalytic systems in the active state. The interaction of ceria surfaces with CO_2 has been investigated both on powder

[a] *Department of Chemistry and Chemical Engineering – Competence Centre for Catalysis, Chalmers University of Technology, Gothenburg, 412 96, Sweden. E-mail: andreas.schaefer@chalmers.se*

[b] *Division of Synchrotron Radiation Research, Lund University, Box 118, SE-221 00 Lund, Sweden*

[c] *Institute of Solid State Physics, University of Bremen, Otto-Hahn-Allee 1, D-28359 Bremen, Germany*

[d] *MAPEX Institute for Materials and Processes, University of Bremen, D-28359 Bremen, Germany*

This journal is © the Owner Societies 2018

Phys. Chem. Chem. Phys., 2018, **20**, 19447–19457 | 19447

supports and model surfaces. Studies on powder catalysts show that a partially reduced cerium oxide support can be re-oxidized by CO_2 to $CeO_{1.8–1.9}$.[12,13] The oxygen is supplied by the dissociation of CO_2 at sites on the metal particles and Ce^{3+} sites in reduced ceria.[14] A study on a $CeO_x(111)$ film by Lykhach et al., however, revealed that neither the presence of a transition metal nor hydroxyl groups is required for the re-oxidation of ceria up to $CeO_{1.90}$ to take place, even at room temperature.[15] It has to be noted that, while the re-oxidation of the oxide has been observed in case of the (111) oriented surface, the (100) and (110) surfaces of CeO_{2-x} have been shown to not be re-oxidized by adsorbed CO_2,[16,17] though exhibiting a strong interaction with CO_2 at low temperature.

Many transition metal surfaces have been employed for the growth of ceria films and structures, of which the three most studied are Ru(0001), Cu(111), and Pt(111). The growth on several substrates has recently been reviewed by Rodriguez et al.[6] and preparation methods as well as the surface chemistry of ceria have been reviewed by Mullins.[16] Rhodium is a transition metal relevant in heterogeneous catalysis, and few studies[18–22] have dealt with ceria films prepared on it. Like on many other transition metal surfaces, cerium oxide films on Rh(111) can either be grown by reactive physical vapor deposition (RPVD), i.e. evaporation of cerium metal in an oxygen ambient,[18] or by deposition of cerium metal onto the substrate and post-annealing in oxygen.[20] It has been demonstrated that the oxide grows in double layers, with one layer being a O–Ce–O tri-layer, and that films of higher thickness are thermally more stable up to 900–1073 K.[18,20] After preparation, the oxide films are reported to possess a stoichiometry close to CeO_2 with a Ce^{3+} content of only a few percent, while thin films are found to exhibit a higher Ce^{3+} content,[22,23] probably due to the proximity to the metal substrate.[24] A question we address with this study is to what extent the difference in reducibility between thin and thick films/islands is reflected in the re-oxidation behavior. In a recent study Grinter et al. showed that ceria islands, which had previously been reduced using a focused X-ray beam, can be re-oxidized by oxygen chemisorbed on the Rh(111) support once the oxygen becomes mobile above 400 K.[21]

In this article we show that the latter effect can be exploited by using the reactivity of the Rh surface at elevated temperatures to split the CO_2 molecule. Operando XPS measurements in the high-vacuum range (10^{-5} hPa) reveal that chemisorbed oxygen and CO are generated during the reaction and that the adsorbed oxygen atoms can then re-oxidize reduced ceria islands. Not surprisingly, this effect is the most effective above the desorption temperature of CO. The results, however, further reveal a temperature dependence of the re-oxidation process that does not depend on the adsorbate coverage, but on the thickness of the ceria islands.

2 Experimental

2.1 Sample preparation

The Rh(111) single crystals (Surface Preparation Laboratory) were cleaned by cycles of Ar^+ sputtering (1–1.5 keV, 20 min) and

annealing (up to 1570 K), including an annealing step in 1×10^{-6} mbar oxygen to remove carbon impurities. The sample surface was considered clean when the signals of C KLL and O KLL emissions were below the detection limit in Auger electron spectroscopy (AES). Additionally, the surfaces were checked by scanning tunneling microscopy (STM) and low energy electron diffraction (LEED) prior to the oxide deposition. The CeO_2 films were prepared by reactive physical vapor deposition (RPVD), i.e. evaporation of Ce metal from a Mo crucible by an electron beam evaporator (EFM3, FOCUS GmbH) in an oxygen background pressure of 1.3×10^{-7} hPa. The growth rate was about 0.4 Å min^{-1}. The substrate temperatures were chosen to be 1030 K and 830 K to control the island sizes. As has been shown for different metal surfaces, a higher substrate temperature initially leads to larger CeO_2 structures, which then quickly grow in height rather than to wet the metal surface.[25,26] A lower growth temperature, on the other side, leads to the growth of a larger number of smaller islands. In fact, it has been shown that continuous CeO_2 films with only a few open layers can be prepared by starting the deposition at lower substrate temperature and increasing the temperature slowly during growth.[27]

The amount of deposited material was determined by evaluating the attenuation of the Rh KLL signal at 300 eV electron energy in AES, assuming an inelastic mean free path of 7.6 Å for the calculation (determined following ref. 28). Together with information from STM we were then able to estimate the total amount of deposited material in monolayer equivalent (MLE) with one monolayer referring to the height of a O–Ce–O trilayer in the [111] direction of the CeO_2 bulk unit cell (3.12 Å).

After preparation, the samples were characterized by AES, STM and LEED before they were taken out of the vacuum chamber and packed in evacuated containers for transport. Hence, the samples were exposed to atmosphere for about 30–40 min in total (including the time needed to mount the samples again). After the samples have been transferred into the vacuum chamber at beamline 9.3.2 at the ALS, spectra were measured before a cleaning procedure was applied. The cleaning procedure consisted of heating the sample to 870 K in 1.3×10^{-5} hPa oxygen. This procedure removes all carbon contamination. Spectra of the as-transferred and clean surface are compiled in Fig. S3 in the ESI.†

2.2 Photoelectron spectroscopy

The reduction and re-oxidation experiments were carried out at the soft X-ray AP-XPS beamline 9.3.2 at the Advanced Light Source in Berkeley, CA, USA.[29] The photons originate from a bending magnet and the end-station is housing a Scienta R4000 HiPP system for operando studies in a pressure up to several hPa. The available photon energy at this beamline ranges from 200 to 900 eV, which renders the Ce 3d levels unavailable for the measurement. Furthermore, also the oxidation state sensitive resonant enhancement of the Ce 4f and O 2p emission in the valence band when exciting with photon energies of the Ce $N_{IV,V}$ transition,[30–32] in the range of 121–125 eV, is not available in the photon energy range provided by the beamline. Hence we measured the Ce 4d levels to determine the oxide's

19448 | Phys. Chem. Chem. Phys., 2018, 20, 19447–19457

This journal is © the Owner Societies 2018

stoichiometry. The procedure is described in detail in the ESI.†
We tested for beam induced reduction by measuring Ce 4d
spectra continuously for 30 min but could not detect any
decrease of the Ce^{4+}-related signal. This is in line with studies
of ceria surfaces by other authors conducted at the same
setup.[33] The Ce 4d spectra were measured with a photon energy
of 450 eV. The photoionization cross section for the 4d level
undergoes a Cooper minimum at lower photon energies,[34,35]
hence a higher photon energy has to be chosen. At 450 eV
photon energy we expect to probe the whole of the CeO_x island
structures in our experiment. The O 1s spectra were recorded at
650 eV photon energy, the C 1s and Rh 3d spectra at 435 eV. The
spectra presented were normalized to the background at
the low binding energy side. Deconvolution of the O 1s and
Rh $3d_{5/2}$ spectra was done using a Doniach-Šunjić profile and a
Shirley-type background (linear for O 1s). The binding energy
scale was calibrated to the Fermi edge of the Rh substrate.

2.3 Temperature measurement

During preparation of the oxide film the temperature was
measured by a type-K thermocouple spot-welded to the
side of the rhodium crystals, which were heated by electron
bombardment from the back side. For the photoelectron
spectroscopy measurements a type-K thermocouple was pressed
by a ceramic piece on the top sides of the hat-shaped crystals,
which were placed on a BN heater. During those measurements
we expect an error not larger than ±10 K for the temperatures
reported in this work.

3 Results

For this study two Rh(111) crystals containing differently
sized CeO_2 islands were prepared by reactive physical vapor
deposition as described in the experimental section. Sample A
contained cerium oxide with a total coverage corresponding
to 2.0 O–Ce–O monolayer equivalents (MLE) while sample B
was covered by 0.9 MLE of the oxide. The total coverage was
estimated by measuring the attenuation of the Rh KLL signal in
AES right after preparation together with the information obtained
by STM (see below). The subsequently recorded LEED images
(Fig. S1, ESI†) show that the oxide grows in (111) orientation in
registry with the substrate, as it has been reported for the
growth on numerous transition metal substrates.[6]

The morphology of the oxide deposit was investigated using
STM. The oxide preferably nucleates as three-dimensional islands
rather than wetting the substrate (Volmer–Weber growth) under
the used growth conditions, as it has also been reported in several
studies on other metal substrates.[26,27,36,37] The micrographs in
Fig. 1 show oxide islands found on the respective samples
(additional images are comprised in Fig. S2, ESI†). Fig. 1(a) shows
a large triangular island of sample A of more than 100 nm in
diameter, grown at 1030 K. The height profile reveals an initial
step height of about 0.95 nm corresponding to three O–Ce–O
trilayers. On top of these first layers several non-closed layers
formed, which consist of smaller islands. The height of the island
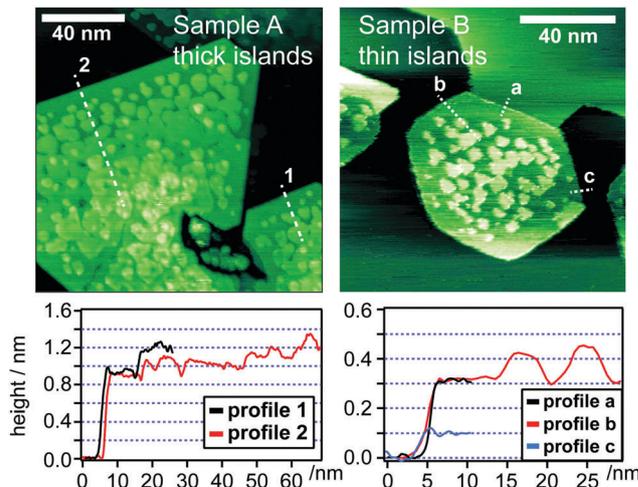

Fig. 1 STM images of ceria islands grown on Rh(111). Left: Sample A: large
triangular island grown at 1030 K. The height profiles below show, that the
initial step is three O–Ce–O trilayers high. Smaller structures nucleate on
top up to 5–6 trilayers in total height. Right: Island grown at 830 K. The
base of the island is only one trilayer high, as the profiles indicate.
A second layer has started to nucleate. Imaging conditions: 600 mV
sample bias, 600 pA.

increases toward its center and up to 5–6 layers in maximum
height can be observed. The smaller islands found on sample B
(Fig. 1(b)) are of hexagonal shape and less than 100 nm in
diameter. The height of the island in Fig. 1(b) is one tri-layer,
with a second layer nucleating on top. The amount of the
second layer observed on the islands varies, and some islands
have larger sections covered by a complete second layer (see
Fig. S2, ESI†). The apparent height of additional layers of the
oxide appears lower than the expected value of about 3 Å due to
reduced tunneling for thicker layers of CeO_2. The apparent
height is further a function of the tunneling bias as has been
reported for biases below 1 V for ceria grown on Pt(111).[36]

Given the signal attenuation in AES and the estimated
average island heights from STM, it can be deduced that both
samples exhibit a comparable amount of uncovered Rh surface
(40 ± 2.5% for the thin and 35 ± 5% for the thick islands). The
same is inferred by the intensities of the diffraction spots
in LEED, which show comparable intensity for oxide and
substrate spots, respectively, in both cases. We will come back
to the amount of exposed Rh surface when discussing the PES
results. In the following, we will refer to the large islands of
samples A as 'thick islands' while the islands in sample B will
be referred to as 'thin islands'.

3.1 Thermal reduction

To follow the change in stoichiometry during annealing
of the oxidized CeO_2 structures of sample A (thick islands),
we measured Ce 4d spectra while heating the sample up
to 920 K (890 K for the thin islands) in a stepwise fashion.
Fig. 2 shows the Ce 4d spectra before (bottom) and after
(top) thermal reduction of both samples. The middle panel of
Fig. 2 shows the evolution of the spectra during reduction of
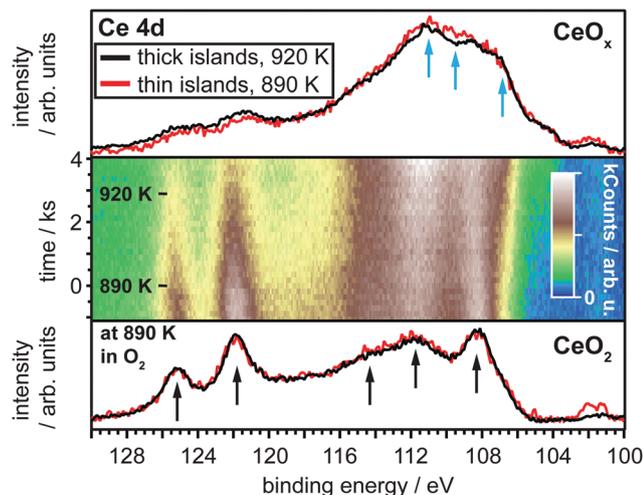the thick islands.

Fig. 2 Bottom: Ce 4d spectra recorded after annealing the ceria structures in oxygen. Arrows point to features indicative of Ce^{4+}. Middle: 2D plot of individual Ce 4d spectra of the thick islands recorded while heating the sample. Top: Spectra recorded after the thermal reduction. Blue arrows indicate features characteristic for Ce^{3+}.

The bottom two spectra before the reduction were measured in the presence of 1.3×10^{-5} hPa oxygen. They exhibit typical features associated with the presence of Ce^{4+} (indicated by arrows). Especially the two peaks at 122 and 125 eV stand out and are thought of to mainly originate from the Ce $4d^9O\ 2p^64f^0$ final state configuration[38] and hence are expected to decrease in intensity with a decrease in Ce^{4+} content in the oxide. The spectra of the oxidized thick and thin islands look virtually identical, inferring an identical oxidation state. It has to be noted, that previous studies of the growth of thin ceria layers on Rh(111) report a stoichiometry of $CeO_{1.84}$ for the first trilayer and a stoichiometry close to CeO_2 for a film of mainly two trilayers thickness.[20,22] The higher concentration of Ce^{3+} ions in the first O–Ce–O trilayer is thought to either originate from a charge transfer from the metal substrate to the cerium ions or by actual oxygen vacancies. However, the cited measurements were done in ultrahigh vacuum, while an oxygen ambient was present during the acquisition of the bottom two spectra in Fig. 2. The oxygen probably hinders the apparent reduction of the very thin oxide layers and may explain why both our films show an identical Ce 4d spectrum for the thin and thick islands in Fig. 2. We hence assume both, thick and thin islands to be CeO_2, i.e. close to 100% Ce^{4+}, in our case.

To reduce the ceria islands thermally, the temperature was held at 870 K after the cleaning treatment and the oxygen was pumped out of the chamber. The final pressure during the following heat treatment was reached after 3–4 spectra, i.e. $\approx 500–700$ s, and stabilized at $1.3–3.0 \times 10^{-9}$ hPa. The temperatures were held constant and only increased at the points indicated in the middle section of Fig. 2, while Ce 4d spectra were acquired. Increasing the temperature to 890 K and 920 K, respectively, took 1–2 spectra, corresponding to 175–350 s. The temperature was kept below 900 K for the thinner islands and close to 900 K for the thicker islands to avoid decomposition

of the oxide, which has been reported to occur above this temperature range.[18,20]

Heating of the ceria structures clearly leads to a decrease of the intensity of the Ce^{4+} related components. At the same time the intensity of features between 107–112 eV increases, indicating an increasing Ce^{3+} concentration. (corresponding data for the thin islands in Fig. S4, ESI†) The samples were heated until no changes were observed any longer in the 4d spectra. The top two spectra in Fig. 2 show the result after the samples have been heated to the respective temperature for at least 30 min. The spectra, again, appear similar, though the thin islands are likely reduced a bit more, indicated by the lower intensity between 119–126 eV and the slightly higher intensity between 108–112 eV.

In order to determine the average stoichiometry of the oxide structures during thermal reduction a linear combination of the most reduced and most oxidized spectrum can be applied to describe every intermediate spectrum. The method has been successfully applied to Ce 3d spectra[39,40] and we describe our approach for the Ce 4d spectra in detail in the ESI.† The results of the evaluation are compiled in Fig. 3 showing the obtained x in CeO_x on the right ordinate and the weight of the CeO_2 spectrum in the linear combination on the left ordinate (for details see ESI†). As is evident from Fig. 3, the reduction starts at 870 K for the thin islands, i.e. right after the oxygen has been closed off, while a temperature of 890 K is necessary for an observable reduction to commence in case of the thick islands. A change of the slope of the decrease of Ce^{4+} is visible at 890 K for the thin islands, which also reach their maximum reduced state after about one hour of annealing time. The thicker islands, however, require a higher temperature and/or a longer time for reduction. The maximum reduced state reached in our experiment is about $CeO_{1.62}$ after more than 60 min of total annealing time.
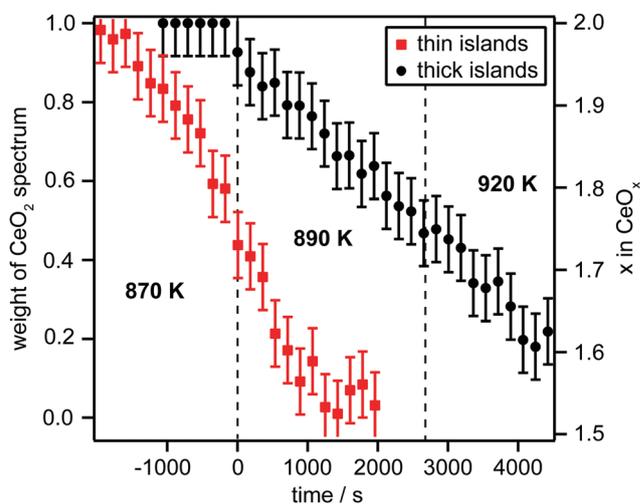

Fig. 3 Result of fitting series of Ce 4d spectra measured during thermal reduction of the thin (red squares) and thick (black circles) ceria islands. Left ordinate: weight of the CeO_2 reference spectrum in the final fit. Right ordinate: resulting stoichiometry for CeO_x with error bars ± 0.04. The time is arbitrarily set to 0 where the thick islands start to reduce. The thin islands were completely reduced at 893 K and not heated further.

19450 | Phys. Chem. Chem. Phys., 2018, 20, 19447–19457

This journal is © the Owner Societies 2018

3.2 Re-Oxidation by CO_2

To investigate to which extent the ceria nanostructures can be re-oxidized when exposed to carbon dioxide, two sets of experiments where performed. In a set of static experiments, the reduced ceria structures were first exposed to 10^{-5} hPa CO_2 at 370 K and then a set of spectra was recorded (still in CO_2 ambient) when no changes were observed any longer (steady state). Subsequently, the temperature was increased stepwise up to 870 K and the same set of spectra was measured at each step. In a dynamic experiment, Ce 4d spectra where measured continuously while the reduced ceria structures where exposed to 10^{-5} hPa CO_2 at a specific temperature.

Static experiment. After the reduction experiment described above the samples were cooled down to 370 K, which was chosen over room temperature as a starting temperature to avoid a long waiting time to achieve thermal equilibrium. Once the temperature was stabilized, 1.3×10^{-5} hPa CO_2 were dosed into the chamber. The samples were kept at the specific temperature for about 20–30 min, until no further changes were discernible in measured Ce 4d spectra. A full set of O 1s, C 1s, Rh 3d, and Ce 4d spectra was measured during CO_2 exposure, before the temperature was increased to the next step.

Before the discussion of information gained from the individual core levels we consider the resulting stoichiometry extracted from the Ce 4d spectra (Fig. 4). After cooling down to 370 K the reduced CeO_x structures exhibited a stoichiometry of $CeO_{1.63}$ and $CeO_{1.61}$ for the thick and thin islands, respectively. That means that a slight re-oxidation already took place when cooling down the sample to 374 K likely caused by residual O_2 gas in the chamber background. Another cause of the observed re-oxidation could be residual water in the chamber background. Studies of water adsorption on partially reduced ceria have, however, not sh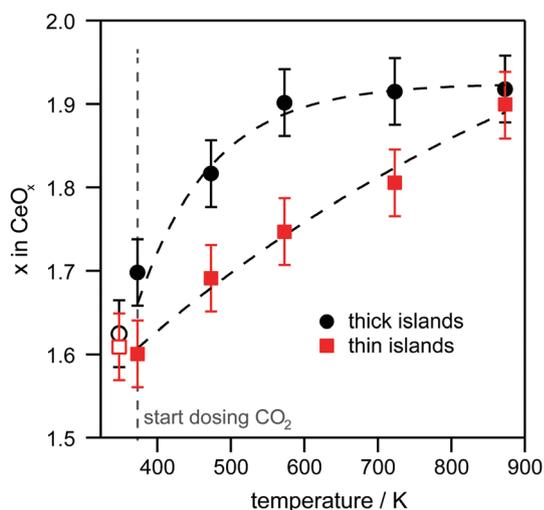own a pronounced re-oxidizing effect and, in some cases, even an increase in the Ce^{3+} signal.[41] The formation of two O–H groups upon water dissociation on the oxide surface should not lead to a higher Ce^{4+} content. Furthermore, O–H groups can be stable up to 500 K on reduced ceria,[16] implying that a re-oxidizing effect of water should only be expected at elevated temperature. We can, however, not completely rule out a slight re-oxidizing effect of residual water in case of our strongly reduced ceria islands.

After dosing 1.3×10^{-5} hPa CO_2 the thick islands oxidize on average to $CeO_{1.70}$ while the oxidation state of the thin islands stays virtually unchanged. Increasing the temperature to 470 K leads to oxidation for both kinds of islands to $CeO_{1.82}$ for the thick and $CeO_{1.70}$ for the thin islands. Already at 570 K the thick islands reach a value of $CeO_{1.90}$ which is not increasing further with increasing temperature. The thin islands are oxidized to just $CeO_{1.75}$ at 570 K and $CeO_{1.81}$ at 720 K before they also reach a value close to $CeO_{1.90}$ at 870 K.

Striving to obtain a better understanding of the difference in the temperature dependence of the oxidation of the two different CeO_x island types, we next consider the other core levels, starting with the C 1s spectra, Fig. 5. At 370 K small amounts of carbon close to the detection limit are observed on both samples, which have likely been collected from the chamber background when cooling down the samples after reduction. When dosing 1.3×10^{-5} hPa CO_2 at 370 K three signals can be resolved in the C 1s spectra of both surfaces. The leading peak is located at 286.3 eV and caused by CO adsorbed on the exposed Rh surface, clearly showing that CO_2 dissociates. The CO related signal exhibits a very similar intensity on both surfaces inferring that both samples contain a comparable area of exposed Rh surface, already assumed earlier. The leading peak further exhibits a small shoulder at the low binding energy side, which cannot clearly be assigned but likely stems from CO bound to three-fold hollow or bridge sites.[42] A signal at 290.0 eV likely originates from carbonate species (CO_3^{2-}).[43,44] The signal is slightly less intense on the sample

Fig. 4 Stoichiometry (x in CeO_x) as a function of sample temperature during CO_2 exposure. Data points left of the dashed line were measured at 370 K in UHV. Filled circles: resulting stoichiometry for the thick islands at the temperature given. Red squares: stoichiometry for the thin islands. Dashed curves are inserted to guide the eye.
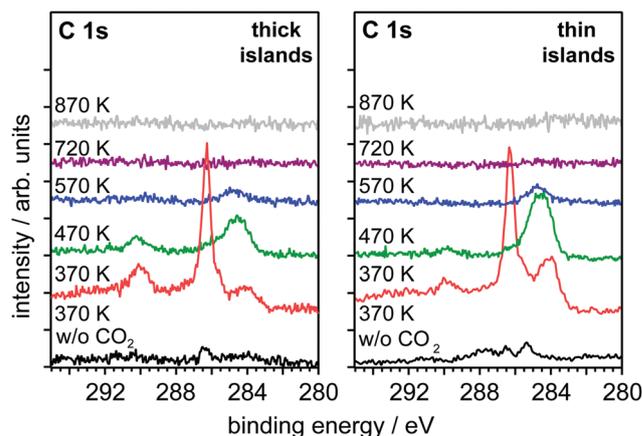
Fig. 5 Carbon 1s spectra during CO_2 exposure. Left: Spectra for the thick oxide islands. Right: Spectra for the thin islands. The samples were kept for 20–30 min at the temperature indicated before a spectrum was recorded. The bottom spectrum was measured at 370 K in UHV after cooling down from the thermal reduction.

containing the thin islands. The third signal at the lowest binding energy, 284.1 eV, falls in the range between CH_x and C species.[45] The signal is more intense for the thin islands, suggesting, that the respective carbon species is bound to the perimeter of the oxide islands. Given that about the same surface area is covered by oxide on the both samples, as the results presented so far show, more perimeter sites are expected to be available on the sample containing smaller islands, thus leading to the higher intensity for the signal at 284.1 eV in case of the thin islands.

Increasing the sample temperature to 470 K leads to a nearly complete disappearance of the CO signal. Only slight intensity is remaining at the position of the former shoulder of the CO signal. The results match reports in literature in which CO desorption has been observed at temperatures close to 500 K on Rh(111).[46,47] The signal located at the lowest binding energy increases in intensity and shifts to higher binding energy when the temperature is increased. This can be interpreted as hydrogenation to $-CH_x$ species and eventually $-CH_3$, as already observed for ceria islands on copper exposed to an CO_2/H_2 mixture.[45] In our case, the hydrogen would have to originate from the chamber background or $-OH$ groups formed on the ceria by spurious amounts of water (e.g. formed at the hot filament of pressure gauges during oxygen dosage). As Fig. 4 shows, only limited re-oxidation is observed at 470 K. A possible explanation for the limited re-oxidation is thus that the sites at which oxygen could enter the ceria islands, the perimeter sites, are still partially blocked by carbon species, significantly hindering the re-oxidation through that channel. When the temperature is increased further to 570 K the $-CH_x$ species start to desorb from the surface and at the same time a further re-oxidation of the ceria islands is observed in both cases. At 720 K and onwards no carbon is detected anymore on either sample.

Selected spectra of the Rh 3d core level are compiled in Fig. 6 (full set in Fig. S6, ESI†). The spectra recorded at 370 K in UHV can be deconvoluted into two peaks originating from a bulk and a surface related signal which are marked B and S in Fig. 6. The binding energy difference of the two components is 0.4 eV, i.e. slightly smaller than the reported value of 0.5 eV for clean Rh(111).[48] The relative integral intensity of the surface and bulk components is shown in panel (c) of Fig. 6 for each annealing step. Before dosing CO_2 the intensity of the surface component is about 16% larger for the sample containing the thin islands, i.e. that sample may exhibit a respective larger amount of exposed Rh surface, which aligns well with the estimations made earlier based on AES and STM.

Dosing CO_2 at 370 K significantly attenuates the surface components in both spectra (middle section of Fig. 6(a) and (b)). At the same time a slight increase in intensity of the bulk signal occurs. This can be explained by CO adsorption on the Rh surface essentially resulting in a shifted surface signal moving underneath the bulk signal as described in ref. 42. The experimental resolution is, in our case, not large enough to discern this extra contribution. The explanation by adsorbed CO is in line with the C 1s spectra showing a large signal
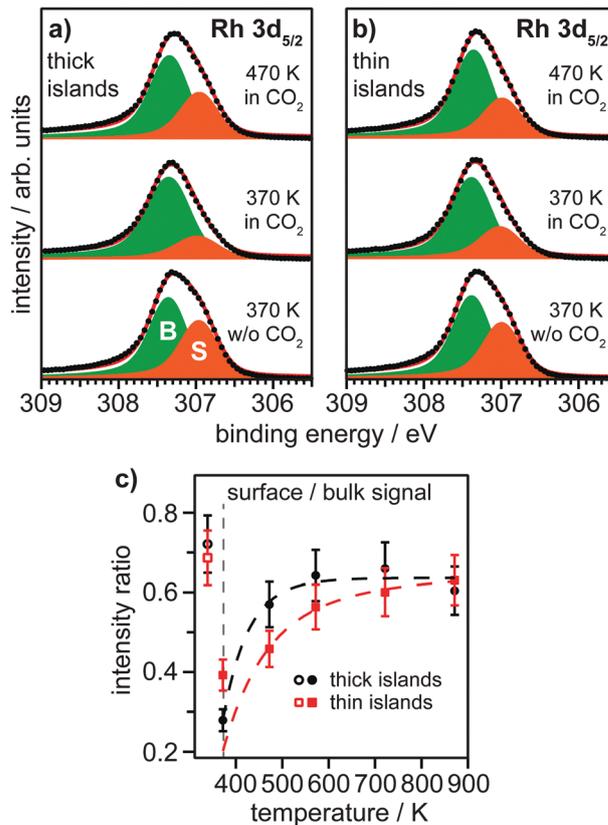

Fig. 6 Selected Rh $3d_{5/2}$ spectra recorded right before and during CO_2 exposure. (a) Sample A containing thick CeO_x islands and (b) sample B containing thin islands. The signals are deconvoluted into two peaks originating from bulk atoms (green, labeled B) and surface atoms (orange, labeled S). (c) Integral intensities of the surface components as a function of sample temperature. Data points left of the dashed line are measured at 370 K before dosing CO_2. The dashed curves are inserted as a guide to the eye.

attributed to CO–Rh at this temperature. However, more surface signal appears to remain for sample B (thin islands). Increasing the temperature to 470 K leads to a recovery of the surface component, also matching the loss of CO–Rh signal, i.e. desorption of CO, in the carbon spectra. At 570 K there is a further recovery of the surface component on sample B while only an insignificant increase occurs for sample A (thick islands). No significant changes occur within the margin of error of the experiment when increasing the temperature further. Finally, the surface to bulk ratio levels out at a similar value for both surfaces.

As the last part of the static experiment we turn to the O 1s spectra, of which a selection is presented in panels (a) and (b) of Fig. 7 (full set in Fig. S7 in ESI†). The deconvolution of spectra measured at 370 K prior to CO_2 exposure reveals three components. The most intense component is located at 529.9 eV and 529.7 eV for the thick and thin islands, respectively. The signal originates from oxygen atoms of the oxide lattice. The binding energy values agree with reported values for reduced ceria.[20] The component at the highest binding energy (532.0 eV) in the two bottom spectra of Fig. 7 originates from species collected when cooling the sample down to 370 K after thermal reduction. A likely assignment are OH groups formed from
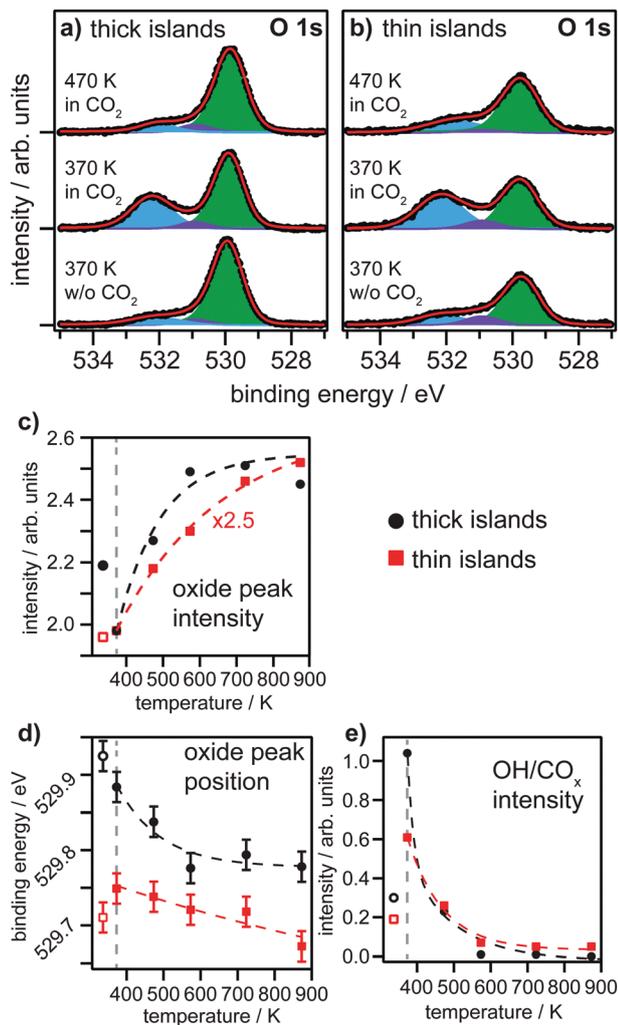
19452 | Phys. Chem. Chem. Phys., 2018, 20, 19447–19457

This journal is © the Owner Societies 2018

Fig. 7 Selected oxygen 1s spectra recorded before and during CO_2 exposure. Spectra are deconvoluted into three peaks. Green: oxide related peak; light blue: OH/CO_3^{2-}; purple: island perimeter/interface. Overall spectra for the (a) thick and (b) thin islands behave similar and corresponding to observations made in the C 1s spectra. (c) Integral intensity of the oxide signal as a function of sample temperature. (d) Position of the oxide peak as function of sample temperature. (e) Integral intensity of the OH/CO_x-related component (blue).

water in the chamber background. Hydroxyl groups have been reported to be present up to 500–700 K on stoichiometric and reduced ceria, respectively.[41] To obtain a satisfying fit of the spectra a third component located at 531 eV was inserted. This signal has previously been interpreted as stemming from Rh–O–Ce entities.[20] We hence also assign this signal to stem from Rh–O–Ce entities, likely located at the perimeter and interface sites of the ceria islands, because the component is observed under all conditions throughout the whole experiment.

Dosing CO_2 at 370 K leads to a signal at 532.2 eV on both samples. Given the results presented so far, the signal must comprise contributions from CO, carbonate, and probably also a minor amount of hydroxyl groups, which cannot be resolved in the O 1s spectra. The same signal decreases again when heating to 470 K, in line with the decrease of CO and CO_3^{2-} intensity in the C

1s spectra. Accordingly, no significant signal is observed anymore at 570 K and onwards at 532 eV as is also shown in panel (e) in Fig. 7 comprising the integral intensity of the component.

A closer look at the integral intensity of the oxide related O 1s signal reveals a temperature dependent increase of the intensity during CO_2 exposure which follows the same trends observed for the stoichiometry extracted from the Ce 4d spectra. In other words: the intensity of the oxide signal of the thick islands reaches a maximum already at 570 K while the temperature needs to be increased up to 870 K for the thin islands to reach a comparable intensity. In general, information about the oxidation state of the oxide structures may also be extracted from the binding energy position of the oxide O 1s signal. Usual values, if reported, range from 530 eV for Ce_2O_3 to 529 eV for CeO_2. The absolute binding energies, however, vary with substrate used and film thickness studied,[16,20,22] while a comprehensive summary of binding energy positions and underlying effects is up to now still lacking. Considering the shift of the position of the oxide related signal upon re-oxidation with CO_2, we only observe a shift of -0.15 and -0.08 eV for the thick and thin islands, respectively (Fig. 7(d)). A shift on the O 1s signal as small as 0.3 eV between CeO_2 and Ce_2O_3 has, for instance, also been reported for films on $SrTiO_3$, while usual values on thicker ceria films on metal substrates, measured in UHV, are in the range of up to 1 eV. The general trend, however, which we observe for the shift in binding energy of the oxide peak during re-oxidation with CO_2 follows all other results reported above. For the thick islands the oxide peak shifts downward by 0.15 eV, indicating oxidation, and reaches a maximum shift at 570 K. For the thin islands the starting binding energy is lower and the downward shift observed is close to the margin of error of the evaluation (shift about 0.08 eV).

Dynamic experiment. In order to follow the dynamics, a second re-oxidation experiment was done, starting at 570 K instead of 370 K, in 1.3×10^{-5} hPa CO_2. Ce 4d spectra were measured continuously during the whole experiment. Fig. 8 compiles the
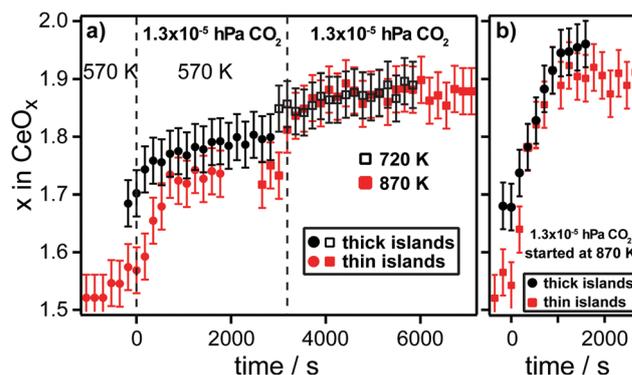

Fig. 8 Stoichiometry extracted from the Ce 4d spectra recorded during the dynamic experiment. Black circles and open squares represent values obtained from the thick islands, and red circles and squares values from the thin islands, respectively. At time 0 s CO_2 was dosed into the chamber. (a) After reduction the sample is cooled to 570 K and then CO_2 is dosed for 3000 s before the temperature is increased to 720 K (thick islands) and 870 K (thin islands), respectively. (b) Samples were kept at 870 K after reduction and CO_2 directly dosed at that temperature.

This journal is © the Owner Societies 2018

Phys. Chem. Chem. Phys., 2018, **20**, 19447–19457 | **19453**

stoichiometry extracted by fitting each Ce 4d spectrum with a linear combination of spectra from the most oxidized and reduced spectrum obtained by thermal reduction (see above section). Also in this experiment a slight re-oxidation already takes place while cooling the samples down to 570 K after reduction, caused by the residual gas in the chamber. Before starting to dose CO_2, the thin islands had re-oxidized to $CeO_{1.57}$ and the thick islands to $CeO_{1.68}$, which, in both cases, is an offset of +0.05 in x compared to the final values after reduction at 870/920 K.

Dosing CO_2 at 570 K leads to a fairly quick increase of the oxygen content in the thin ceria structures corresponding to $CeO_{1.74}$ after 700 s (see red circles in Fig. 8(a)). Further CO_2 exposure does not lead to further oxidation. Increasing the temperature to 870 K, which was accomplished within 350 s corresponding to two measured Ce 4d spectra, a stoichiometry of $CeO_{1.89}$ is reached after a time of 1600 s CO_2 exposure at 870 K. From there on even additional 2500 s of exposure do not oxidize the thin ceria islands further, in accordance with the static experiment.

After a rather quick oxidation to $CeO_{1.75}$ within 500 s at 570 K the thick islands oxidize further rather slowly within the following 1200 s up to $CeO_{1.80}$ (black circles in Fig. 8(a)). The data does not clearly indicate that a final value has been reached after a total CO_2 exposure of about 3000 s, which again is in accordance with the static experiment showing that a longer exposure at 570 K already leads to a final stoichiometry close to $CeO_{1.90}$ for the thick islands. However, in the dynamic experiment the temperature was increased to 720 K after 3000 s CO_2 exposure at 570 K. The temperature increase also leads to a nearly immediate increase of the Ce^{4+} content in the thick islands corresponding to a stoichiometry of $CeO_{1.84}$ which increases slowly further to $CeO_{1.89}$ over the course of 2000 s. Both samples end up at the same stoichiometry of $CeO_{1.90}$ as it has been observed in the static experiment.

In a last experiment, the oxide structures were reduced and then exposed to CO_2 directly at 870 K (Fig. 8(b)). Also in this case the zero in the time scale marks the start of CO_2 dosing. For both, thin and thick islands, a steep increase in Ce^{4+} content is observed. The thin islands stabilize to $CeO_{1.91}$ after about 850 s while the thick islands reach $CeO_{1.94}$ within 1000 s (again note that one spectrum takes 175 s to measure).

4 Discussion

The thermal reduction in UHV shows that the thin islands of one to two O–Ce–O trilayer thickness are more reducible than thicker islands. This effect also has been described for ceria islands and films on Pt(111).[24] The authors of ref. 20 observe the onset of reduction already at about 770 K while a thicker film (10 ML) only contains one monolayer equivalent of Ce^{3+} ions even after heating to 1020 K. The higher reducibility of the thin islands in ref. 20 is reasoned by a decrease in the surface oxygen vacancy formation energy. Furthermore, the authors report a change in the electronic structure of ultra-thin ceria films on Pt which are caused by their dimensionality and the proximity of the platinum substrate. Also Castellarin-Cudia

et al. report a difference in the electronic structure of the first ceria trilayer grown on Rh(111), which is further shown in LDOS calculations.[49] The calculations in ref. 49 reveal a non-zero electron density in the gap, while the results also show that the second O–Ce–O trilayer already screens the substrate effectively. Our experimental results suggest that the increased reducibility is an effect that scales with film thickness to some extent. The thicker islands, which are four to six O–Ce–O trilayers in height, clearly exhibit a lower reducibility while they are still more reducible than thicker films as, for example, in ref. 24. It has to be noted that PES is an averaging technique. Especially regarding the thick islands it cannot be excluded that thinner parts, as they are shown by STM to exist at the outer areas of the islands, exhibit a lower oxygen content, while the thicker areas are re-oxidized above $CeO_{1.90}$. Nevertheless, the trends when going from smaller, thinner toward larger, thicker ceria structures are evident. A more precise method like resonant PES at the Ce 4d edge[30–32] would be necessary to determine the Ce^{3+} content in the very first layers more accurately. To compare very surface sensitive studies with spectra carrying more information from the lower layers of the oxide seems to be even more important in light of predictions from theory[50,51] and recent experimental results,[52] suggesting, that oxygen vacancies at $CeO_2(111)$ surfaces migrate to a subsurface position, while they stay at the surface at other surface orientations. The effect described by the authors in ref. 52 is likely also essential for the activation of CO_2 over ceria catalysts and further study is required in this field.

Exposure to CO_2 clearly re-oxidized the reduced ceria structures up to $CeO_{1.90}$. $CeO_{1.90}$ appears to be an upper limit even when increasing the temperature up to 870 K in 1.3×10^{-5} hPa CO_2. Studies by Matolin *et al.* showed that closed ceria films on Cu(111) that have been partially reduced to $CeO_{1.80}$ can be re-oxidized to $CeO_{1.90}$ by dosing about 30 000 L CO_2 at room temperature.[53] It is pointed out in ref. 53 that partially reduced ceria(111) surfaces exhibit an intrinsic reactivity towards CO_2, evidenced by the fact that re-oxidation occurs in the absence of transition metal particles or hydroxyl groups on the ceria. The upper limit of $CeO_{1.90}$ of the re-oxidation was explained by a decrease in oxygen vacancy formation energy that occurs when the oxygen content in the ceria increases. In our experiment it takes an equivalent dose of about 8000 L at 570 K until a rather stable stoichiometry is reached for both island types. From there on, the oxidation state increases only slowly for the thick islands but even after a total dose of 30 000 L it has only a stoichiometry of $CeO_{1.80}$, as shown in the dynamic experiment. An increase of the sample temperature is needed to speed up the re-oxidation process. An even higher total dose, compared to the static experiment, of approximately 50 000 L (a third each at 370 K, 470 K, and 570 K) leads to $CeO_{1.90}$ at 570 K. Thus, the total CO_2 dose required to reach a stoichiometry of $CeO_{1.90}$ below 570 K is much higher compared to the dose needed for a continuous cerium oxide film at room temperature.[53] However, at 870 K sample temperature a much lower dose of 10 000 L is sufficient to reach $CeO_{1.90}$ for both kinds of islands. Hence we conclude that in our experiment the re-oxidation is facilitated

19454 | *Phys. Chem. Chem. Phys.*, 2018, **20**, 19447–19457

This journal is © the Owner Societies 2018

through two pathways: (1) the decomposition of CO_2 on the oxide itself leads to direct re-oxidation as described in ref. 53, but appears to be less effective below ≈ 600 K. If this were, however, the main process, we would expect a re-oxidation already at the lower temperatures of our study, i.e. 370 K and 470 K, respectively. We do not observe significant re-oxidation at those temperatures. Hence we propose that (2) in the main process CO_2 decomposes on the exposed Rhodium surface providing atomic oxygen species that are able to diffuse to the ceria islands and are incorporated into the oxide lattice. It has been debated under which conditions CO_2 dissociates on rhodium.[54–56] We do observe a signal in the C 1s spectrum that can be assigned to CO–Rh(111), and it disappears at temperatures typical for CO desorption.[46] Hence we conclude that CO_2 indeed dissociates to CO and O on the Rh surface. As it has been demonstrated in ref. 21, reduced ceria islands can be re-oxidized by chemisorbed oxygen on Rhodium above 400 K, i.e. when the temperature is high enough for the oxygen to become mobile and being incorporated into the ceria islands. However, even at 470 K we do not observe the maximum re-oxidation in the static experiment. As the C 1s spectra reveal, this is caused by CO adsorbed on the rhodium surface, likely hindering the diffusion of oxygen to the islands and/or the adsorption of further CO_2 to a significant extent. Once the CO has left the rhodium surface and the island-Rh perimeter sites, which happens between 400 and 570 K, the re-oxidation of the oxide proceeds. The results discussed above reflect the characteristics of a bifunctional catalyst. The CeO_x/Rh surface is capable of activating (splitting) CO_2 at rather low temperatures below 400 K. Temperatures above 400 K then facilitate the migration of oxygen to the reduced oxide islands while the remaining CO is potentially available for further reaction with, e.g. hydrogen to form products like methanol or methane, as seen in other model systems.[6,11,57] However, a reactivation step is required to keep the CeO_x islands in a partially reduced state for oxygen capture.

The adsorbed CO does not, however, explain the different temperatures needed to oxidize the thick and thin islands to $CeO_{1.90}$. From both surfaces the carbon species desorb in the same temperature range. But only when reaching 870 K have the thin islands been oxidized to the same extent as the thick islands. Furthermore, the C 1s and Rh 3d spectra indicate that both surfaces exhibit a comparable amount of free Rh surface area, which implies that in both cases comparable amounts of oxygen are supplied for the re-oxidation of the CeO_x structures. From the results discussed we conclude that the higher reducibility observed for the thin islands is an intrinsic property. Our data does not provide further insight into the underlying effects, but it is likely that an electronic effect, as discussed in ref. 24 and 49, caused by the proximity to the metal substrate is at the origin of the higher reducibility and, in turn, the higher temperatures required for the re-oxidation observed for the thin islands.

5 Conclusions

In this article we have shown that ceria nanostructures deposited on a rhodium substrate can be re-oxidized by exposure to CO_2 after initial thermal reduction. Not only does the reducibility but also the re-oxidizability by CO_2 depend on the thickness of the ceria deposit. Ultrathin ceria islands are found to reduce at lower temperatures and are more difficult to re-oxidize while islands of several O–Ce–O trilayers in thickness require higher temperature for reduction and are more easily re-oxidized. Consistent with previous reports on the reducibility of ceria ultrathin films this effect appears to be caused by the proximity to the metal substrate, and we have demonstrated here that it applies to the re-oxidation by CO_2 as well. The maximum oxidation state of strongly reduced CeO_x achievable by re-oxidation using CO_2 is close to an average stoichiometry of $CeO_{1.90}$, even with the assistance of an exposed rhodium surface, and thus lower than the maximum achieved by molecular oxygen. The reason for this result partly remains an open question and calls for further studies.

The CO_2 mainly acts a an oxygen source for the re-oxidation of the CeO_x islands. Nevertheless, the CeO_x/Rh system efficiently removes oxygen from CO_2, transforming it to CO at rather low temperatures. In the presence of hydrogen, these CO species can potentially undergo further reactions to form industrially relevant products like methane, as was recently reported for a Rh/CeO_x powder catalyst.[57]

The possibility to tune the reducibility of small oxide deposits by controlling the structure's dimensionality and materials combination appears especially interesting in view of small oxide deposits on transition metals in form of nanoparticles or -porous structures, so called inverse catalysts or in janus or dumbbell like particles in which both, metal and oxide, are nano-sized.[58] Furthermore, the inverse configurations of thin oxide layers covering metal particles or structures are likely of importance for a variety of present and future catalytic systems. In general, obtaining an understanding of the interaction of CO_2 with different surface orientations of pure and doped ceria films, also at conditions more relevant to catalytic applications, remains an essential step towards the rational design of catalysts for CO_2 utilization.

Conflicts of interest

There are no conflicts of interest to declare.

Acknowledgements

This journal is © the Owner Societies 2018

Phys. Chem. Chem. Phys., 2018, **20**, 19447–19457 | 19455

References

1 A. Trovarelli and P. Fornasiero, *Catalysis by ceria and related materials*, Imperial College Press, 2nd edn, 2013.

2 T. Montini, M. Melchionna, M. Monai and P. Fornasiero, *Chem. Rev.*, 2016, **116**, 5987–6041.

3 A. Rangaswamy, P. Sudarsanam and B. M. Reddy, *J. Rare Earths*, 2015, **33**, 1162–1169.

4 F. P. Leisenberger, S. Surnev, G. Koller, M. G. Ramsey and F. P. Netzer, *Surf. Sci.*, 2000, **444**, 211–220.

5 J. A. Rodriguez, P. Liu, J. Graciani, S. D. Senanayake, D. C. Grinter, D. Stacchiola, J. Hrbek and J. Fernández-Sanz, *J. Phys. Chem. Lett.*, 2016, **7**, 2627–2639.

6 J. A. Rodriguez, D. C. Grinter, Z. Liu, R. M. Palomino and S. D. Senanayake, *Chem. Soc. Rev.*, 2017, 1824.

7 T. Lunkenbein, J. Schumann, M. Behrens, R. Schlögl and M. G. Willinger, *Angew. Chem., Int. Ed.*, 2015, **54**, 4544–4548.

8 J. Graciani, K. Mudiyanselage, F. Xu, A. E. Baber, J. Evans, S. D. Senanayake, D. J. Stacchiola, P. Liu, J. Hrbek, J. Fernández Sanz and J. A. Rodriguez, *Science*, 2014, **345**, 546–550.

9 S. Kattel, P. J. Ramírez, J. G. Chen, J. A. Rodriguez and P. Liu, *Science*, 2017, **355**, 1296–1299.

10 R. M. Palomino, P. J. Ramírez, Z. Liu, R. Hamlyn, I. Waluyo, M. Mahapatra, I. Orozco, A. Hunt, J. P. Simonovis, S. D. Senanayake and J. A. Rodriguez, *J. Phys. Chem. B*, 2017, **122**, 794–800.

11 S. D. Senanayake, P. J. Ramírez, I. Waluyo, S. Kundu, K. Mudiyanselage, Z. Liu, Z. Liu, S. Axnanda, D. J. Stacchiola, J. Evans and J. A. Rodriguez, *J. Phys. Chem. C*, 2016, **120**, 1778–1784.

12 T. Jin, Y. Zhou, G. J. Mains and J. M. White, *J. Phys. Chem.*, 1987, **91**, 5931.

13 K. Otsuka, Y. Wang, E. Sunada and I. Yamanaka, *J. Catal.*, 1998, **175**, 152.

14 S. Bernal, G. Blanco, J. M. Gatica, C. Larese and H. Vidal, *J. Catal.*, 2001, **200**, 411.

15 Y. Lykhach, T. Staudt, R. Streber, M. P. A. Lorenz, A. Bayer, H. P. Steinrück and J. Libuda, *Eur. Phys. J. B*, 2010, **75**, 89.

16 D. R. Mullins, *Surf. Sci. Rep.*, 2015, **70**, 42.

17 C. Yang, F. Bebensee, J. Chen, X. Yu, A. Nefedov and C. Wöll, *Chem. Phys. Chem.*, 2017, **18**, 1874.

18 S. Eck, C. Castellarin-Cudia, S. Surnev, M. G. Ramsey and F. P. Netzer, *Surf. Sci.*, 2002, **520**, 173.

19 S. Eck, C. Castellarin-Cudia, S. Surnev, K. C. Prince, M. G. Ramsey and F. P. Netzer, *Surf. Sci.*, 2003, **536**, 166.

20 L. H. Chan and J. Yuhara, *J. Chem. Phys.*, 2015, **143**, 074708.

21 D. C. Grinter, C. Muryn, A. Sala, C. M. Yim, C. L. Pang, T. O. Mentes, A. Locatelli and G. Thornton, *J. Phys. Chem. C*, 2016, 11037.

22 L. H. Chan and J. Yuhara, *Surf. Sci.*, 2017, 69.

23 J. I. Flege, J. Höcker, J. T. Sadowski, S. D. Senanayake and J. Falta, Nucleation, morphology, and structure of sub-nm thin ceria islands on Rh(111), *Surf. Interface Anal.*, accepted.

24 G. Gasperi, L. Amidani, F. Benedetti, F. Boscherini, P. Glatzel, S. Valeri and P. Luches, *Phys. Chem. Chem. Phys.*, 2016, **18**, 20511.

25 M. Sauerbrey, J. Höcker, M. Wellbrock, M. Schowalter, J.-O. Krisponeit, K. Müller-Caspary, A. Rosenauer, G. Wei, L. Colombi Ciacchi, J. Falta and J. I. Flege, *Cryst. Growth Des.*, 2016, **16**, 4216.

26 D. C. Grinter, S. D. Senanayake and J. I. Flege, *Appl. Catal., B*, 2016, **197**, 286.

27 F. Dvořák, O. Stetsovych, M. Steger, E. Cherradi, I. Matolínová, N. Tsud, M. Škoda, T. Skála, J. Mysliveček and V. Matolín, *J. Phys. Chem. C*, 2011, **115**, 7496.

28 S. Tanuma, C. J. Powell and D. R. Penn, *Surf. Interface Anal.*, 2005, **37**, 1–14.

29 M. E. Grass, P. G. Karlsson, F. Aksoy, M. Lundqvist, B. Wannberg, B. S. Mun, Z. Hussain and Z. Liu, *Rev. Sci. Instrum.*, 2010, **81**, 053106.

30 V. Matolín, M. Cabala, V. Cháb, I. Matolínová, K. C. Prince, M. Škoda, F. Šutara, T. Skála and K. Veltruská, *Surf. Interface Anal.*, 2008, **40**, 225–230.

31 V. Matolín, I. Matolínová, L. Sedláček, K. C. Prince and T. Skála, *Nanotechnology*, 2009, **20**, 215706.

32 V. Matolín, J. Libra, M. Škoda, N. Tsud, K. C. Prince and T. Skála, *Surf. Sci.*, 2009, **603**, 1087–1092.

33 Z. Liu, T. Duchoň, H. Wang, D. C. Grinter, I. Waluyo, J. Zhou, Q. Liu, B. Jeong, E. J. Crumlin, V. Matolin, D. J. Stacchiola, J. A. Rodriguez and S. D. Senanayake, *Phys. Chem. Chem. Phys.*, 2016, **18**, 16621.

34 M. Baron, O. Bondarchuk, D. Stacchiola, S. Shaikhutdinov and H. J. Freund, *J. Phys. Chem. C*, 2009, **113**, 6042.

35 J. W. Cooper, *Phys. Rev.*, 1962, **128**, 681.

36 P. Luches, F. Pagliuca and S. Valeri, *J. Phys. Chem. C*, 2011, **115**, 10718.

37 B. Kaemena, S. D. Senanayake, A. Meyer, J. T. Sadowski, J. Falta and J. I. Flege, *J. Phys. Chem. C*, 2013, **117**, 221.

38 D. R. Mullins, S. H. Overbury and D. R. Huntley, *Surf. Sci.*, 1998, **409**, 307.

39 H. Wilkens, O. Schuckmann, R. Oelke, S. Gevers, M. Reichling, A. Schaefer, M. Baumer, M. H. Zoellner, G. Niu, T. Schroeder and J. Wollschlager, *Phys. Chem. Chem. Phys.*, 2013, **15**, 18589.

40 A. Allahgholi, J. I. Flege, S. Thieß, W. Drube and J. Falta, *Chem. Phys. Chem.*, 2015, **16**, 1083.

41 Y. Lykhach, V. Johánek, H. A. Aleksandrov, S. M. Kozlov, M. Happel, T. Skála, P. S. Petkov, N. Tsud, G. N. Vayssilov, K. C. Prince, K. M. Neyman, V. Matolín and J. Libuda, *J. Phys. Chem. C*, 2012, **116**, 12103.

42 A. Beutler, E. Lundgren, R. Nyholm, J. N. Andersen, B. Setlik and D. Heskett, *Surf. Sci.*, 1997, **371**, 381.

43 S. D. Senanayake and D. R. Mullins, *J. Phys. Chem. C*, 2008, **112**, 9744.

44 S. D. Senanayake, D. Stacchiola, J. Evans, M. Estrella, L. Barrio, M. Pérez, J. Hrbek and J. A. Rodriguez, *J. Catal.*, 2010, **271**, 392.

45 Z. Zuo, P. J. Ramírez, S. D. Senanayake, P. Liu and J. A. Rodriguez, *J. Am. Chem. Soc.*, 2016, **138**, 13810.

46 L. A. DeLouise and N. Winograd, *Surf. Sci.*, 1984, **138**, 417.

47 G. Krenn, I. Bako and R. Schennach, *J. Chem. Phys.*, 2006, **124**, 144703.

19456 | *Phys. Chem. Chem. Phys.*, 2018, **20**, 19447–19457

This journal is © the Owner Societies 2018

48 J. N. Andersen, D. Hennig, E. Lundgren, M. Methfessel, R. Nyholm and M. Scheffler, *Phys. Rev. B: Condens. Matter Mater. Phys.*, 1994, **50**, 17525.

49 C. Castellarin-Cudia, S. Surnev, G. Schneider, R. Podlucky, M. G. Ramsey and F. P. Netzer, *Surf. Sci.*, 2004, **554**, L120.

50 M. V. Ganduglia-Pirovano, J. L. F. Da Silva and J. Sauer, *Phys. Rev. Lett.*, 2009, **102**, 1–4.

51 G. E. Murgida and M. V. Ganduglia-Pirovano, *Phys. Rev. Lett.*, 2013, **110**, 246101.

52 C. Yang, X. Yu, S. Heissler, P. Weidler, A. Nefedov, Y. Wang, C. Wöll, T. Kropp, J. Paier and J. Sauer, *Angew. Chem., Int. Ed.*, 2017, **56**, 16399–16404.

53 T. Staudt, Y. Lykhach, N. Tsud, T. Skála, K. C. Prince, V. Matolín and J. Libuda, *J. Catal.*, 2010, **275**, 181.

54 L. H. Dubois and G. A. Somorjai, *Surf. Sci.*, 1980, **91**, 514.

55 D. W. Goodman, D. E. Peebles and J. M. White, *Surf. Sci. Lett.*, 1984, **140**, L239.

56 H. A. C. M. Hendrickx, A. P. J. M. Jongenelis and B. E. Nieuwenhuys, *Surf. Sci.*, 1985, **154**, 503.

57 N. M. Martin, P. Velin, M. Skoglundh, M. Bauer and P.-A. Carlsson, *Catal. Sci. Technol.*, 2017, **7**, 1086–1094.

58 S. Jiang and S. Granick, *Janus Particle Synthesis, Self-Assembly and Applications*, The Royal Society of Chemistry, 1st edn, 2012.

This journal is © the Owner Societies 2018

Phys. Chem. Chem. Phys., 2018, **20**, 19447–19457 | **19457**